Article

Performance Estimation and Selection Guideline of SiPM Chip within SiPM-Based OFDM-OWC System

Long Zhang, Rui Jiang *, Xinke Tang [ID]**, Zhen Chen, Zhongyi Li and Juan Chen**

Peng Cheng Laboratory, Shenzhen 518055, China
* Correspondence: jiangr01@pcl.ac.cn

Abstract: The orthogonal frequency division multiplexing (OFDM), which has high spectral efficiency, is an attractive solution for silicon photomultiplier (SiPM)-based optical wireless communication (OWC) systems to boost data rates. However, the currently available SiPMs are not optimized for implementing the OFDM receiver. Incorporating different types of SiPM at the OFDM receiver results in different data rates at the same condition. Therefore, the receiver designer requires a method for predicting the performance of SiPMs and then selects the best one to build the optimum receiver. In this paper, we first investigate the origin of SiPM's power-dependent frequency response. The investigation outcome is then used to create a method for predicting the subcarrier SNR. Combining the estimated subcarrier SNR with the bit-loading scheme, we finally propose a general approach for estimating the fundamental OFDM data rate an SiPM chip can support at a given received power. Results are then presented that can be used by the future receiver designer as a guideline to find the best type of SiPM to build the optimum OFDM receiver.

Keywords: silicon photomultiplier; optical wireless communication; OFDM

1. Introduction

Optical wireless communication (OWC), which uses the unlicensed spectrum to provide high-speed wireless communication, is expected to play an important role in the 6G network [1]. The OWC system requires a highly sensitive photodetector [2]. The P-i-N photodiode (PIN PD) and avalanche photodiode (APD) are the commonly used photodetectors in OWC. Unfortunately, the PIN has no internal gain, and the APD generates excess shot noise, which limits their sensitivity. SiPM is an array of single-photon avalanche diodes (SPAD) with an internal gain larger than 10^6 and without excess noise [3,4]. Results show that the sensitivity of SiPM can approach the Poisson limit, which is significantly more sensitive than the two commonly used PDs in OWC [4,5]. With this advantage, incorporating SiPM in the OWC receiver can significantly improve the OWC system's achievable SNR at the same received power. However, SiPM suffers from dead time, during which the fired SPAD microcell is unable to detect another incident photon [3,4]. The dead time generates a nonlinear output response and a bandwidth limit, both of which limit the data rate that the SiPM-based receiver can achieve [5].

OFDM, which modulates the quadrature amplitude modulation (QAM) symbols on the orthogonal subcarriers, has a high spectral efficiency [6]. Using OFDM in an SiPM-based OWC system can maximize its achievable data rate. It has been demonstrated that the data rate that the SiPM-based OFDM-OWC system can support varies from 500 Mbps to 5 Gbps [7]. Although different signal optimization algorithms result in different data rate enhancement, the fundamental performance of an SiPM-based OFDM-OWC system is primarily determined by the SiPM chip used to build the receiver. A receiver designer has to be able to select the best type of SiPM from those that are available. Moreover, if SiPMs become an integral part of OWC receivers, their manufacturers will be interested in optimizing their performance for this sizeable potential market. To help future SiPM and

receiver designers, this paper proposes a general approach to estimate the performance of OFDM receivers that incorporate an SiPM and points out a guideline to select and design the best type of SiPM for implementing the optimum OFDM receiver.

In Section 2, the origin of SiPM's power-dependent frequency response is investigated. A method for estimating the subcarrier SNR is then described in Section 3. In Section 4, an approach developed to estimate the data rate of the SiPM-based OFDM system is presented. The results obtained using this approach to estimate the performance of SiPMs with various numbers of SPADs, recovery time constant, and photon detection efficiency (PDE) are discussed in Section 5. Finally, conclusions are drawn in Section 6.

2. Power-Dependent Frequency Response of SiPM

SiPM has a power-dependent frequency response [8], and hence the frequency resource of an SiPM-based OFDM system can use changes with the received power. To build an accurate approach for estimating SiPM's performance within an OFDM system, the origin of SiPM's power-dependent frequency response has to be understood.

SiPM is a solid-state photon counter which consists of a number of parallel-connected photon-counting microcells. Each microcell includes a SPAD and a quenching resistor. All the microcells within SiPM share a common output. Once a photon is detected, a current pulse generated by the fired microcell is added to the common output. Hence, the total output signal of an SiPM is a sum of the current pulses associated with different fired microcells. At an incident light intensity L, the average number of fired SPAD microcells N_f within observation time T is given by [9]:

$$N_f = \frac{N \times T \times \lambda_{in}}{1 + \lambda_{in} \times \tau} \tag{1}$$

$$\lambda_{in} = \frac{A_{SPAD} \times \eta \times L}{E_{ph}} \tag{2}$$

where N is the total number of SPAD microcells within SiPM, A_{SPAD} is the total area of a single SPAD, E_{ph} refers to the single photon energy, λ_{in} is the arrived photon rate, η refers to the PDE, and τ is the dead time which is 2.2 times the recovery time constant of a single SPAD microcell, τ_d [9].

The most commonly used equivalent circuit model of an SiPM is illustrated in Figure 1 [10,11]. According to the status of each microcell, the SiPM is divided into active and passive components. In the active part, each fired SPAD is modeled as a resistor R_d in parallel with a capacitor C_d. The resistor represents the internal resistance of the diode space-charge and quasi-neutral region, and the capacitor represents the junction capacitance of the inner depletion layer [10,11]. In the passive part, the inactive SPAD is modeled as a capacitor only. The integrated quenching resistor is modeled by a resistor R_q associated with its parallel stray capacitance C_q. The recovery time constant τ_d is given by $\tau_d = R_q(C_d + C_q)$. A further parasitic capacitance C_g across the two-pixel terminals is also introduced in the equivalent model, accounting for the presence of the metal grid paths spanning over the entire surface of the semiconductor device [10]. When N_f photons are detected by an SiPM with N microcells, the resistor and capacitor values in Figure 1 are [10]:

$$
\begin{aligned}
C_{d,N_f} &= C_d \times N_f, & R_{q,N_f} &= \frac{R_q}{N_f}, & C_{q,N_f} &= C_q \times N_f \\
C_{d,N_p} &= C_d \times (N - N_f), & R_{q,N_p} &= \frac{R_q}{(N - N_f)}, & C_{q,N_p} &= C_q \times (N - N_f) \\
R_{d,N_f} &= \frac{R_d}{N_f}
\end{aligned}
\tag{3}
$$

where N_f in the subscript represents the number of fired SPADs corresponding to the active components and N_p in the subscript refers to number of inactive SPADs corresponding to the passive components.
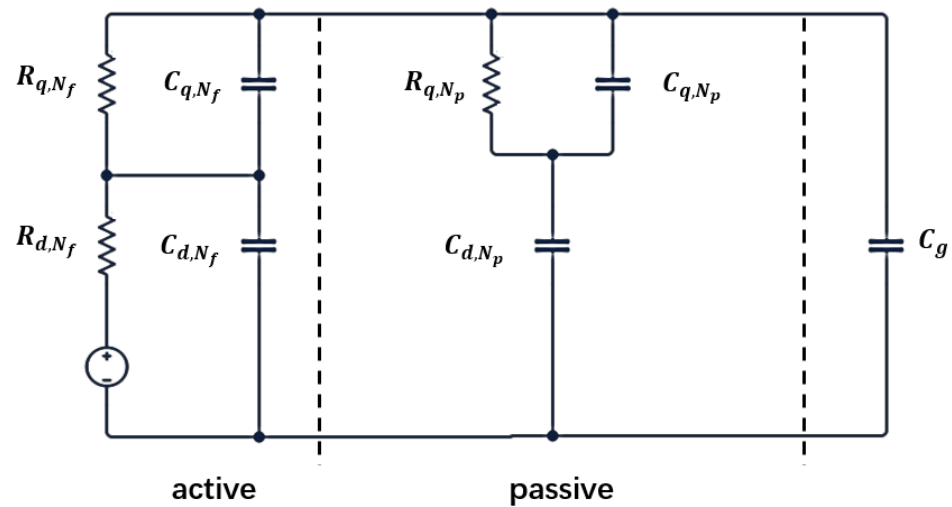
Figure 1. The equivalent circuit of an SiPM chip [10,11].

The transfer function of the SiPM can be modeled by an exponential decay [12]:

$$h(t) = \frac{1}{\tau_s} e^{-\frac{t}{\tau_s}} \tag{4}$$

The frequency response of the SiPM, $1/(j\omega\tau_s + 1)$, is therefore determined by the RC time constant τ_s. For OFDM transmission, the incident light power over the SiPM has to make SiPM's output pulses overlap to form a signal envelope for accurate signal detection. The envelope is proportional to the incident light level which makes the SiPM behave like a highly sensitive APD [3]. Since the output signal is contributed by the fired microcells, no current passing through R_{q,N_p} and hence the passive microcells can be regarded as a parasitic capacitor C_{eq}. The RC constant τ_s can therefore be expressed as:

$$\tau_s = \frac{R_{q,N_f} \times R_{d,N_f}}{R_{q,N_f} + R_{d,N_f}} \times (C_{q,N_f} + C_{d,N_f} + C_{eq} + C_g) \tag{5}$$

where C_{eq} is given by $C_{eq} = \left(C_{d,N_p} \times C_{q,N_p}\right) / \left(C_{d,N_p} + C_{q,N_p}\right)$.

The accuracy of Equation (5) has been validated using an off-the-shelf SiPM (On semiconductor 30035). The RC time constant of the tested SiPM was measured using LD LP520-SF15 and an oscilloscope (MSO7104B). The bandwidth of the tested LD is larger than 1 GHz. In the measurement, the LD is modulated using a rectangular waveform with a frequency of 100 kHz. The purple spots are the measured RC time constant of the tested SiPM at the standard output against different received powers, and the blue curve is the estimated RC time constant based on Equation (5). The detailed parameters of the tested SiPM are listed in Table 1, obtained from [13,14]. Results in Figure 2 suggest that Equation (5) can accurately estimate the power-dependent RC constant. In addition, since τ_s in Equation (4) is a function of the number of fired SPAD microcells, the frequency response of SiPM is power-dependent. With the number of fired SPADs increasing, more diode resistors become parallel and the number of diode parasitic capacitors is reduced, which makes the RC constant become reduced with the increased optical power.

Table 1. Key parameters in simulation [13,14].

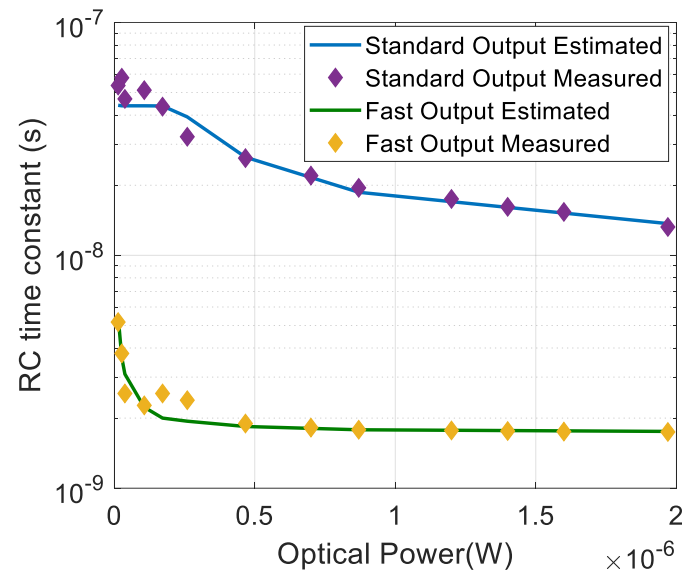| Parameters	Value	Parameters	Value
C_d	160 fF	C_g	10 fF
C_q	11.6 fF	N	5676
R_q	200 kΩ	τ_d	45 ns
R_d	50 Ω	η	22%@520 nm
C_{fast}	2.5 fF	A_{SPAD}	3.07×3.07 mm^2

Figure 2. The measured RC time constant of the tested SiPM at different incident optical power using the standard output and the fast output.

According to the relationship between the 3 dB bandwidth and the RC time constant, $B_{3dB} = 1/(2\pi\tau_s)$ [12], the maximum 3 dB bandwidth of the tested SiPM is limited to ~10 MHz. To improve the time resolution, the manufacturer added a series-connected capacitor C_{fast} at the output, as shown in Figure 3. Because the equivalent diode capacitance is reduced by an order of magnitude, the SiPM using the fast output has a much smaller RC constant than using the standard output. The equivalent diode capacitance is:

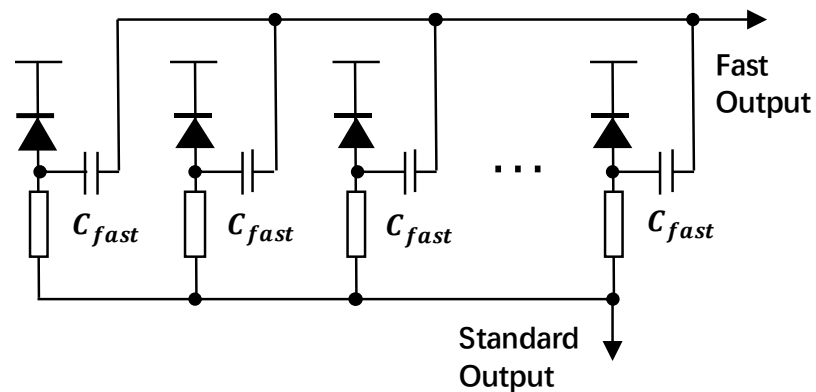$$C_{eq,d} = \frac{C_d \times C_{fast}}{C_d + C_{fast}} \tag{6}$$

Figure 3. Schematic of SiPM with fast output [13].

The yellow spots in Figure 2 are the measured RC time constant of the tested SiPM using the fast output and the green curve shows the estimated RC time constant calculated by Equation (5) after substituting $C_{eq,d}$ into Equation (3). The agreement between the estimated results and the measured data indicate that Equations (4)–(6) can be used to estimate the frequency response of the tested SiPM when fast output has been used. Additionally, compared with the standard output, the 3 dB bandwidth was improved by a factor of 10 when fast output was used.

3. Method of Predicting Subcarrier SNR

For estimating the OFDM data rate, the SNR at each subcarrier is required. The estimated frequency response, which shows the signal power at different frequencies, can be used as prior knowledge for the SNR estimation.

The OFDM signal is a superposition of the modulated subcarriers. Without performing power loading, the transmitted power is equal across subcarriers. Regarding each subcarrier as an independent single carrier transmission, the number of photons detected by SiPM at an individual subcarrier within a sample duration can be estimated by Equation (1). The dominant noise source in an SiPM-based receiver is shot noise [3]. Assuming the channel response is flat, the SNR at each subcarrier can be expressed as [15]:

$$SNR = \frac{N_s}{\sqrt{N_s + N_b}} \qquad (7)$$

where N_s is the number of detected signal photons and N_b is the number of detected background photons. However, in practice, the SNRs at different subcarriers degrade with the increase in frequency due to the channel response. Therefore, Equation (7) can only be valid for estimating the maximum subcarrier SNR.

The frequency response shows the signal power at different frequencies, which is related to the signal counts N_s at the SiPM-based receiver. When the background counts (N_b) are negligible, the SNR at the SiPM-based receiver is close to a square root of N_s according to Equation (7). Therefore, the normalized SNR at the SiPM-based receiver is a square root of the normalized channel gain in frequency response. For generating the optical OFDM signal, the clipping process is required to prevent the negative intensity and the nonlinear distortion at the cost of introducing the clipping noise and distortion, which also affects the subcarrier SNR [16]. Combining the maximum subcarrier SNR, the normalized SNR, and the correction factor caused by clipping, the SNRs at all the subcarriers $SNR(f)$ can be estimated, which is given by:

$$SNR(f) = 10 \times \log_{10} SNR_{\max} + 10 \times \log_{10} \sqrt{F(f)} + \alpha(f) \qquad (8)$$

where $SNR_{\max}$ refers to the maximum subcarrier SNR. $F(f)$ is the normalized frequency response of the whole system which takes the frequency response of all the devices within the system into account. The frequency response of the SiPM at different received power can be estimated using Equations (4) and (5), and the frequency response of other devices can be obtained from the datasheet provided by the manufacturer; $\alpha(f)$ is the correction factor which is related to the impact of clipping. The fundamental performance of an SiPM-based OWC system is determined by the SiPM chip incorporated in the receiver. Optimizing the clipping level will provide additional SNR gain for a given SiPM [7]. Since this work concentrates on figuring out the SiPM chip design and selection guideline instead of investigating the signal optimization method, for simplicity, the clipping level that makes the signal distortion and clipping noise negligible is used in this study. Therefore, $\alpha(f)$ is set to 0 in this work.

In order to verify the accuracy of using Equation (8) for predicting the subcarrier SNR, an experiment was performed. The experimental setup is shown in Figure 4. For simplicity, the DC-biased optical OFDM (DCO-OFDM) is used in this work. Compared with the asymmetrically clipped optical OFDM (ACO-OFDM), DCO-OFDM has higher

spectral efficiency. The DCO-OFDM signal with 512 subcarriers and a cyclic prefix (CP) length of 16 was generated in MATLAB. This signal was conditioned for transmission by clipping any values outside the allowed operating range. The clipping level was set to $\pm 2.5\sigma$ to minimize the signal distortion and noise from clipping [16,17]. The conditioned digital signal was then converted to the analog signal through AWG (AWG5202). The maximum amplitude of the output signal from the AWG was limited to 500 mV. A Mini-circuit ZHL6A+ amplifier with a 3 dB bandwidth of 500 MHz was used to maximize the transmitted signal. Combining with a DC bias (50 mA) at the LD mount, the amplified signal drove a 520 nm LD LP520-SF15 to generate the optical signal. An adjustable optical attenuator was placed after the LD to change the transmitted optical power. To reduce the impact of ambient light, this experiment was conducted in the dark, and a 1 nm optical filter with a 3 mm $\times$ 3 mm aperture was placed over the SiPM. The ambient light measured after the optical filter was less than 2 nW. The output signal from the SiPM's fast output was captured by an oscilloscope (MSO7104B). The captured signal was recovered back to the binary bits after synchronization, fast Fourier transform (FFT), equalization, and M-QAM demodulation. SNR estimation was implemented using the reference pilot symbols modulated in binary phase-shift keying (BPSK). The SNRs at different frequency subcarriers were obtained based on error vector magnitude estimation (EVM) [18].
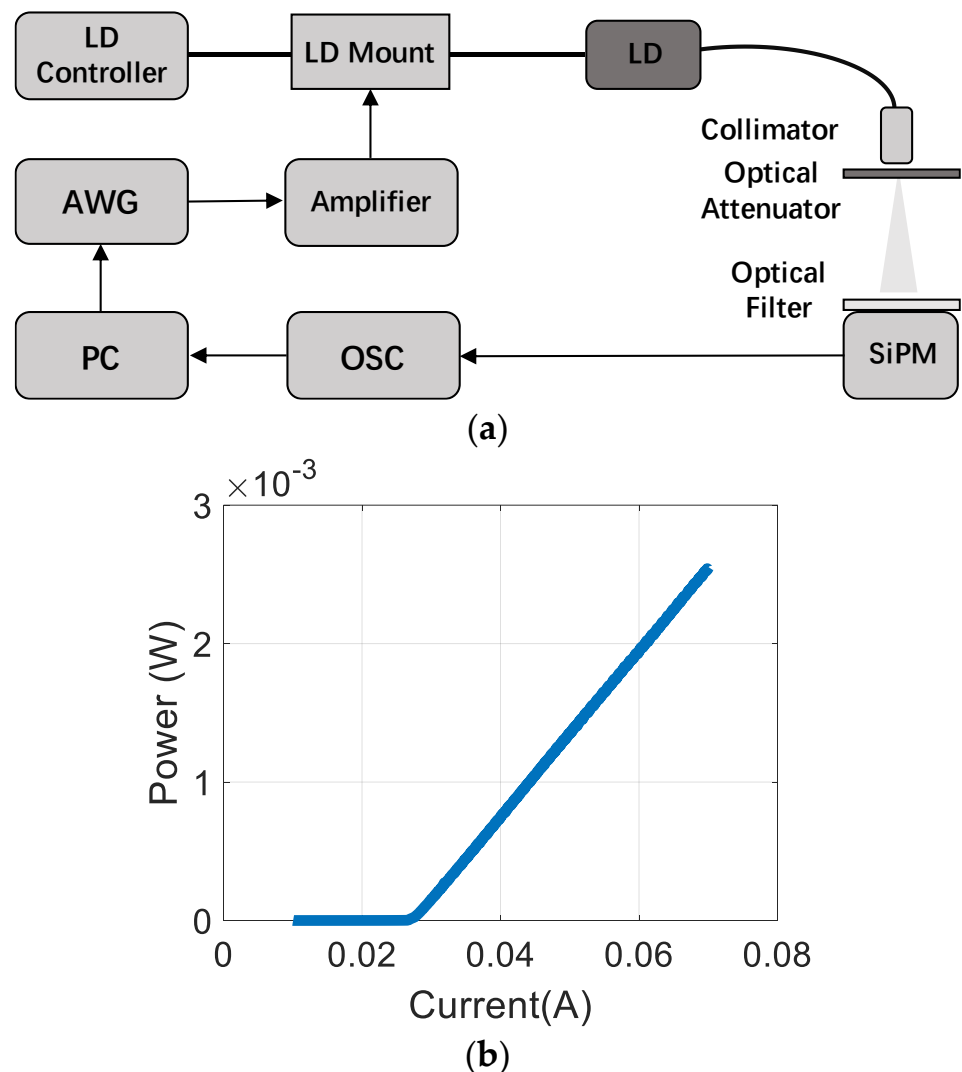

Figure 4. (**a**) Experimental setup (AWG: Arbitrary Waveform Generator, LD: laser diode, OSC: oscilloscope). (**b**) Measured optical power from the tested LD at different bias currents.

The discrete spots in Figure 5 are the measured maximum subcarrier SNRs achieved at various received optical powers. The solid curve in Figure 5 is calculated based on Equation (7). The good agreement between the estimated results and the measured data suggests that Equation (7) can be used to estimate the maximum subcarrier SNR when the clipping levels make the clipping noise and clipping distortion negligible.
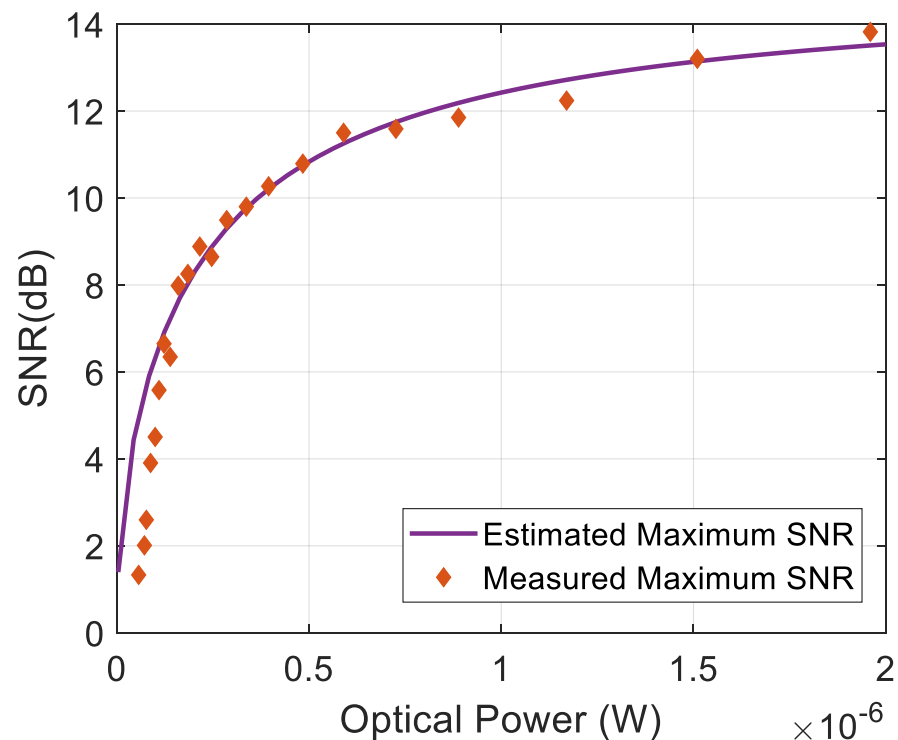

Figure 5. The maximum subcarrier SNR against various received optical power using a clipping level of $\pm 2.5\sigma$.

The dashed curve in Figure 6 shows the estimated SNRs of the tested system at different frequency subcarriers, which are calculated based on Equation (8). In order to obtain an accurate estimation of the tested system's channel response, the frequency response of the amplifier $G_a(f)$ and other electronics $G_o(f)$ used in Figure 4 was also taken into account. The fitting function for the tested amplifier and other electronics is given by:

$$
\begin{aligned}
G_a(f) = a_0 &+ a_1 \times \cos(wf) + b_1 \times \sin(wf) \\
&+ a_2 \times \cos(2wf) + b_2 \times \sin(2wf) \\
&+ a_3 \times \cos(3wf) + b_3 \times \sin(3wf)
\end{aligned}
\tag{9}
$$

$$
G_o(f) = a \times f^b + c
\tag{10}
$$

where f is the frequency and the best fitting values to the measured $G_a(f)$ and $G_o(f)$ in dB are listed in Table 2. The correction factor α is set to 0 since the signal distortion and noise introduced by clipping can be ignored at the clipping level of $\pm 2.5\sigma$ [16]. Results in Figure 6 show that the estimated subcarrier SNR approximately matches the measured results, which suggests that Equation (8) can be used to predict the subcarrier SNR.
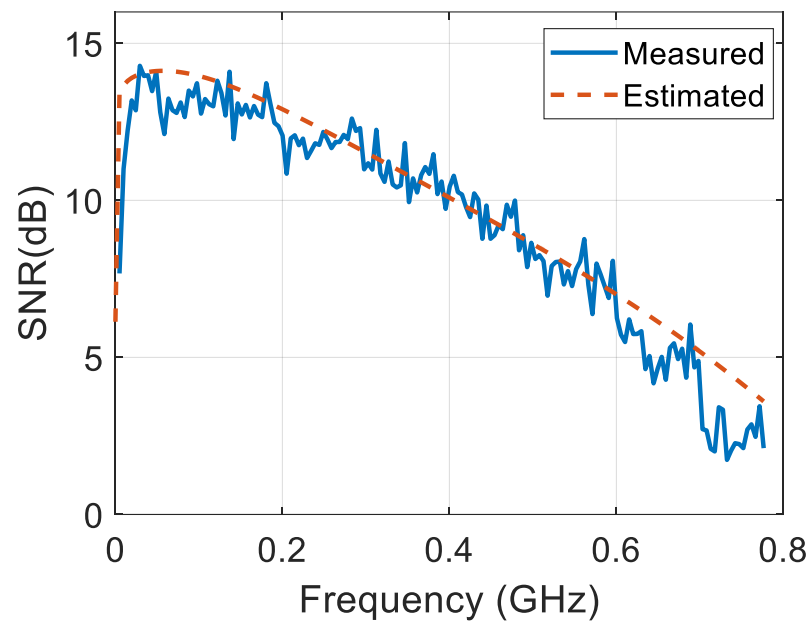
Figure 6. Subcarrier SNR measured at a received optical power of 2 µW using a clipping level of ±2.5σ.

Table 2. Fitting parameters.

Parameters	Value	Parameters	Value
a_0	−30.76	b_3	−3.961
a_1	22.15	w	1.618×10^{-9}
a_2	18.11	a	−61.55
a_3	10.08	b	−0.1706
b_1	−0.5856	c	3.275
b_2	−2.362	-	-

4. Data Rate Estimation and Verification

After applying the bit-loading algorithm to the estimated subcarrier SNR, the achievable OFDM data rate using an SiPM-based receiver can be predicted. The bit-loading process allocates different numbers of bits to the subcarriers according to the subcarrier SNR [18]. The SNR required to obtain a target BER at different QAM sizes is calculated based on Gaussian distribution. After the DFT process, the signal-dependent noise within the SiPM-based receiver becomes signal independent over the frequency subcarrier, making the QAM constellation diagram at each subcarrier also follow the Gaussian distribution [19]. Therefore, the typical bit-loading scheme can be directly used in the SiPM-based OFDM system. In this paper, the Levin–Campello (LC) algorithm is used for bit loading [18]. Table 3 lists the SNRs required by M-QAM to obtain a BER of 3.8×10^{-3}, considering an FEC overhead of 7% [20].

Table 3. SNR required by M-QAM to obtain a BER of 3.8×10^{-3}.

M-QAM	Required SNR (dB)
2-PSK	6.8
4-QAM	9.8
8-QAM	14.4
16-QAM	16.5

The spectral efficiency of the DCO-OFDM system after performing bit loading is given by [17]:

$$E = \frac{\sum_{k=0}^{N_{FFT}/2-1} \text{sgn}(M_k) \log_2 M_k}{N_{FFT} + N_{CP}} \tag{11}$$

where N_{FFT} is the FFT size, M_k is the constellation size on the kth subcarrier after bit loading, N_{cp} is the size of the CP in the time domain, and $sgn(x)$ is the sign function. Then, the system's data rate is:

$$D = 2 \times B \times E \tag{12}$$

where B is the single-sided bandwidth of the system which can be calculated as $B = \frac{1}{2 \times T_s}$ and T_s is the sampling period.

A flow chart representing the approach used to estimate the data rate that an SiPM can support at a given received power with OFDM is shown in Figure 7. This approach starts with inputting the incident light intensity L, sample time T, the specification of a given SiPM of interest, and the frequency response of other devices within the system. Then, the number of SPADs fired within SiPM at a given received power is calculated based on Equations (1) and (2). The frequency response of the SiPM-based receiver achieved at a given received power can then be estimated using Equations (4) and (5). Combined with the maximum subcarrier SNR, the subcarrier SNR is calculated by Equation (8). After applying the bit-loading algorithm, the spectral efficiency and hence the data rate can be predicted based on Equation (12).
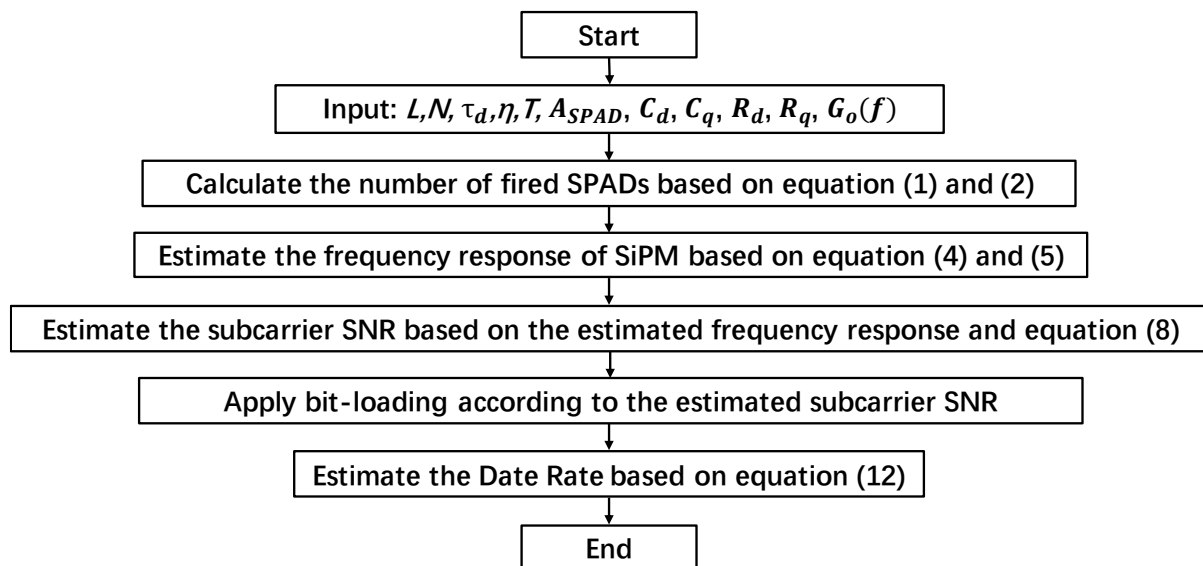

Figure 7. A general approach to estimate the achievable OFDM data rate using a SiPM-based OFDM receiver.

The dashed line in Figure 8 shows the estimated data rates at different received optical power calculated based on the data rate estimation approach shown in Figure 7. Due to that the number of allocated bits at a given subcarrier do not increase linearly with SNR, the dashed curve is not linear. The red spots are the measured results achieved by the tested system shown in Figure 4. The good agreement between the estimated and the measured results suggests that this approach can estimate the OFDM data rate achieved by an SiPM-based receiver at different received optical power.
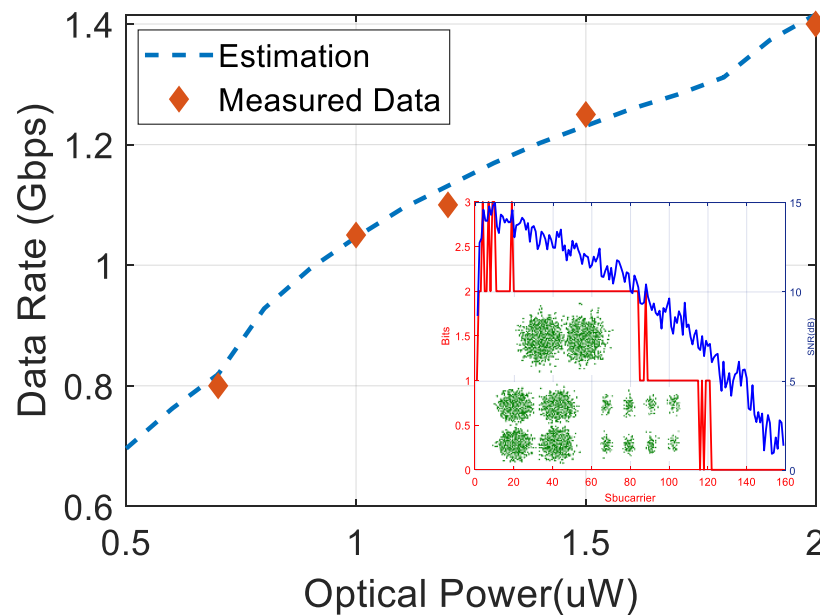
Figure 8. Data rate achieved at different received optical power with bit loading. The inset shows the bits assigned to each subcarrier achieving a data rate of 1.4 Gbps at the received optical power of 2 μW.

5. Discussion

Since SiPMs are a relatively new technology, the newly released product has significantly better characteristics than their predecessors, which offers the prospect of achieving even higher data rates at the same received power. The approach validated in Section 4 is used in this section to investigate the possible performance of SiPMs with a higher number of SPADs, shorter recovery time constant, and higher PDE. In the simulation, the same parameters and system configuration in Figure 4 are used.

Due to that each SPAD microcell is inactive during its dead time, SiPM has a nonlinear response. This nonlinear response limits the subcarrier SNR of the SiPM-based receiver according to Equations (1) and (7). An SiPM with a larger number of SPADs will have more available SPADs to detect the incident photons and hence will be less impacted by the dead time. Increasing the number of SPADs within SiPM can therefore increase the SNR at each subcarrier. However, this approach also reduces the bandwidth of the SiPM due to the increased number of passive microcells and their associated passive capacitance. Figure 9 shows the estimated data rate at a PDE of 22% with various recovery time constants against different numbers of SPADs. Results suggest that the bandwidth reduction is negligible compared with the SNR increment. For example, the SNR is improved by 3 dB at the reduction in the bandwidth by 1% when the number of SPADs increases from 5000 to 20,000. Consequently, increasing the number of SPADs within SiPM eventually boosts the data rate, as shown in Figure 9.

The recovery time constant, which determines the length of dead time, is a function of R_q, C_d, and C_q. Reducing the recovery time constant can therefore reduce SiPM's nonlinearity and increase SiPM's bandwidth simultaneously, according to Equations (1) and (5). At present, the typical recovery time constant of a commercially available SiPM varies from 15 ns to 50 ns [13]. Results in Figure 9 show the possible data rates can be achieved with typical recovery time constant values [13], which confirms that the data rate increases with the reduction in the recovery time constant.
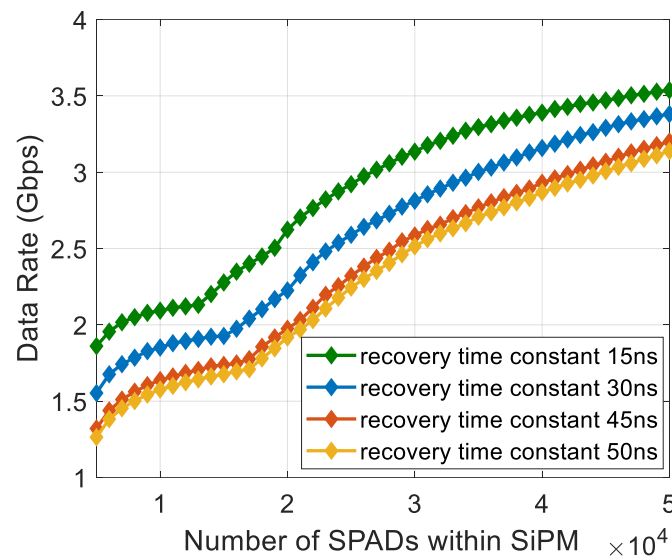
Figure 9. The data rate can be achieved with a larger number of SPADs and a shorter recovery time constant at a PDE of 22% with a received optical power of 2 μW.

Figure 10 shows the estimated data rate against different numbers of SPADs at a recovery time constant of 15 ns with different PDEs. Equation (7) suggests that increasing the number of received signal photon counts can improve the SNR. As a result, increasing SiPM's PDE improves the SNR and hence the achievable data rate at the same received power, as shown in Figure 10. In [7], a commercially available SiPM, which has a peak PDE of 48%, recovery time constant of 15 ns, and contains 1.5×10^4 SPADs, achieved a data rate of 3 Gbps at a received power of 2 μW operated at a PDE of 36% using DCO-OFDM. This experimental result is quite close to our prediction shown in Figure 10. The validated performance improvement confirms that the SiPM with a larger number of SPADs, shorter recovery time, and higher PDE can achieve a higher data rate. When the number of SPADs is higher than 4×10^4, at a recovery time constant of 15 ns and a PDE of 48%, the data rate of the SiPM-based OFDM-OWC system can be higher than 4 Gbps with the same received power. Under the same condition, the data rate that can be supported by conventional PIN is below 500 Mbps, and the typical APD is 3 Gbps [21]. This result suggests that the increased sensitivity made available by the use of SiPM can be exploited to boost the OWC system's data rate.
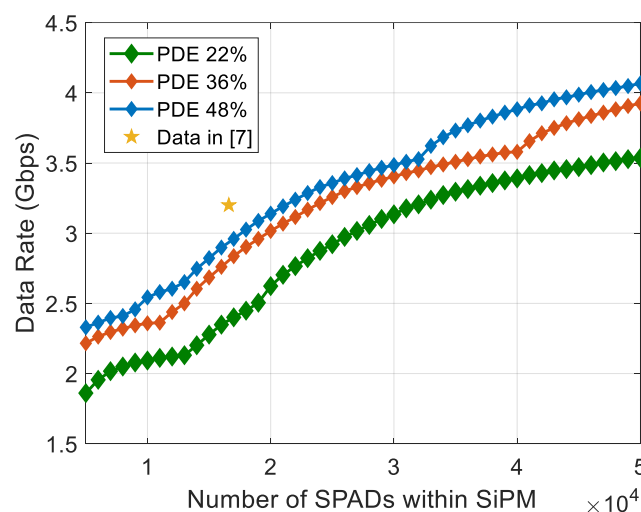

Figure 10. Data rate can be achieved by the SiPM with different PDEs at the received optical power of 2 μW [7].

6. Conclusions

In an SiPM-based OFDM-OWC system, the SiPM chip used at the receiver dominates the achievable data rate. The electrical property of SiPM determines the frequency resource used for transmitting the OFDM symbol, and the nonlinearity of the SiPM determines the subcarrier SNR.

In this paper, a model for estimating the power-dependent RC constant and hence the frequency response of the SiPM was derived according to SiPM's equivalent circuit model and showed to agree with results obtained from a commercially available SiPM. Since the normalized SNR at the SiPM-based receiver is a square root of the normalized channel gain in frequency response, a method for predicting the subcarrier SNR was then presented based on the estimated frequency response and the maximum subcarrier SNR. The subcarrier SNR estimation method validated in the paper was then used to create a general approach for predicting the achievable OFDM data rate using a given SiPM. Results presented in this paper show that this approach accurately predicts the OFDM data rate using an SiPM-based receiver.

The validated estimation approach was then used to predict the performance of SiPMs with a higher number of SPADs, shorter recovery time constant, and higher PDE. The results show that the best type of SiPM to use in OFDM receivers is one with a large number of SPADs, short recovery time constant, and large PDE. An SiPM with 4×10^4 SPADs, 15 ns recovery time, and 48% PDE should be possible to support a data rate of 4 Gbps. Further work is needed to confirm these predictions and to explore the possibility of achieving even higher data rates.

References

1. You, X.; Wang, C.X.; Huang, J.; Gao, X.; Zhang, Z.; Wang, M.; Huang, Y.; Zhang, C.; Jiang, Y.; Wang, J.; et al. Towards 6G Wireless Communication Networks: Vision, Enabling Technologies, and New Paradigm Shifts. *Sci. China Info. Sci.* **2021**, *64*, 1–74. [CrossRef]
2. Chi, N.; Zhou, Y.; Wei, Y.; Hu, F. Visible Light Communication in 6G: Advances, Challenges, and Prospects. *IEEE Veh. Technol. Mag.* **2020**, *15*, 93–102. [CrossRef]
3. Zhang, L.; Chitnis, D.; Chun, H.; Rajbhandari, S.; Faulkner, G.; O'Brien, D.; Collins, S. A Comparison of APD- and SPAD-Based Receivers for Visible Light Communications. *J. Light. Technol.* **2018**, *36*, 2435–2442. [CrossRef]
4. Huang, S.; Patanwala, S.M.; Kosman, J.; Henderson, R.K.; Safari, M. Optimal Photon Counting Receiver for Sub-Dead-Time Signal Transmission. *J. Light. Technol.* **2020**, *38*, 5225–5235. [CrossRef]
5. Li, Y.; Safari, M.; Henderson, R.; Haas, H. Nonlinear Distortion in SPAD-Based Optical OFDM Systems. In Proceedings of the 2015 IEEE Globecom Workshops (GC Wkshps), San Diego, CA, USA, 6–10 December 2015; pp. 1–6. [CrossRef]
6. He, C.; Ahmed, Z.; Collins, S. Signal Pre-Equalization in a Silicon Photomultiplier-Based Optical OFDM System. *IEEE Access* **2021**, *9*, 23344–23356. [CrossRef]
7. Huang, S.; Chen, C.; Bian, R.; Haas, H.; Safari, M. 5 Gbps Optical Wireless Communication using Commercial SPAD Array Receivers. *Opt. Lett.* **2022**, *47*, 2294–2297. [CrossRef] [PubMed]
8. Chen, Z.; Tang, X.; Sun, C.; Li, Z.; Shi, W.; Wang, H.; Zhang, L.; Zhang, A. Experimental Demonstration of Over 14 AL Underwater Wireless Optical Communication. *IEEE Photon- Technol. Lett.* **2021**, *33*, 173–176. [CrossRef]
9. Matthews, W.; Ahmed, Z.; Ali, W.; Collins, S. A 3.45 Gigabits/s SiPM-Based OOK VLC Receiver. *IEEE Photonics Technol. Lett.* **2021**, *33*, 487–490. [CrossRef]

10. Acerbi, F.; Gundacker, S. Understanding and simulating SiPMs. *Nucl. Instrum. Methods Phys. Res. A, Accel. Spectrom. Detect. Assoc. Equip.* **2019**, *926*, 16–35. [CrossRef]
11. Seifert, S.; van Dam, H.T.; Huizenga, J.; Vinke, R.; Dendooven, P.; Lohner, H.; Schaart, D.R. Simulation of Silicon Photomultiplier Signals. *IEEE Trans. Nucl. Sci.* **2009**, *56*, 3726–3733. [CrossRef]
12. Ali, W.; Manousiadis, P.; O'Brien, D.C.; Turnbull, G.; Samuel, I.; Collins, S. A Gigabit VLC receiver that incorporates a flu-orescent antenna and a SiPM. *J. Lightwave Technol.* **2022**, *40*, 5369–5375. [CrossRef]
13. J-Series SiPM Sensors Datasheet, Mar. 2020. Available online: https://www.onsemi.com/pub/Collateral/MICROJ-SERIES-D.PDF (accessed on 10 December 2021).
14. Otte, A.N.; Garcia, D.; Nguyen, T.; Purushotham, D. Characterization of three high efficiency and blue sensitive silicon pho-tomultipliers. *Nucl. Instruments Methods Phys. Res. Sect. A Accel. Spectrometers Detect. Assoc. Equip.* **2017**, *846*, 106–125. [CrossRef]
15. Zappa, F.; Tisa, S.; Tosi, A.; Cova, S. Principles and features of single-photon avalanche diode arrays. *Sens. Actuators A: Phys.* **2007**, *140*, 103–112. [CrossRef]
16. Dimitrov, S.; Sinanovic, S.; Haas, H. Clipping Noise in OFDM-Based Optical Wireless Communication Systems. *IEEE Trans. Commun.* **2012**, *60*, 1072–1081. [CrossRef]
17. Dimitrov, S.; Haas, H. *Principles of LED Light Communications: Towards Networked Li-Fi*; Cambridge University Press: Cambridge, UK, 2015.
18. Tsonev, D.; Chun, H.; Rajbhandari, S.; McKendry, J.J.D.; Videv, S.; Gu, E.; Haji, M.; Watson, S.; Kelly, A.E.; Faulkner, G.; et al. A 3-Gb/s single-LED OFDM-based wireless VLC link using a gallium nitride microLED. *IEEE Photonics Technol. Lett.* **2014**, *26*, 637–640. [CrossRef]
19. Almer, O.; Tsonev, D.; Dutton, N.A.; Al Abbas, T.; Videv, S.; Gnecchi, S.; Haas, H.; Henderson, R.K. A SPAD-Based Visible Light Communications Receiver Employing Higher Order Modulation. In Proceedings of the IEEE Global Communications Conference (GLOBECOM), San Diego, CA, USA, 6–10 December 2015.
20. Forward Error Correction for High Bit-Rate DWDM Submarine Systems. ITU-T Recommendation G.975.1. 2004. Available online: https://www.itu.int/rec/T-REC-G.975.1-200402-I/en (accessed on 10 December 2021).
21. Jukić, T.; Steindl, B.; Zimmermann, H. 400um Diameter APD OEIC in 0.35um BiCMOS. *IEEE Photonics Technol. Lett.* **2016**, *28*, 2004–2007. [CrossRef]